Astron. Astrophys. 357, 301–307 (2000)

ASTRONOMY AND ASTROPHYSICS

Braking of electrons in pulsar magnetospheres by Compton scattering in thermal radiation fields

R. Supper and J. Trümper

Max-Planck-Institut für Extraterrestrische Physik, Postfach 1603, 85740 Garching, Germany

Received 3 December 1999 / Accepted 17 February 2000

Abstract. Electrons accelerated at the polar cap of a pulsar lose energy by interactions with the thermal photospheric radiation. Using Michel's acceleration model (1974) we present an analytical treatement of these braking processes taking into account curvature radiation as well as resonant and non–resonant inverse Compton scattering and the distribution of the thermal photons originating from the polar cap. Results are obtained for a wide range of pulsar parameters. It turns out that for photospheric temperatures below $kT \cong 100\,\mathrm{eV}$ and polar magnetic fields below $B \cong 10^{12.5}$ Gauss braking by inverse Compton scattering has negligible influence on the end energy of the electrons around the polar axes. For magnetic field strength between $10^{12.5}$ and $10^{13.5}$ Gauss the energy loss is significant but depends on the pulsar rotation period. In the case of very high temperatures such as $kT = 1\,\mathrm{keV}$ the energy loss is dramatic within a wide range of magnetic field strengths. Millisecond pulsars are not affected.

Key words: acceleration of particles – radiation mechanisms: thermal – scattering – stars: neutron – stars: pulsars: general

1. Introduction

Electrons accelerated near the polar cap of pulsars interact with the thermal radiation emitted by the photosphere via non–resonant and (cyclotron) resonant inverse Compton collisions (e.g. Kardashev et al. 1984). Several groups have examined how these processes affect the end energies of electrons and the production of gamma rays. For the electron acceleration model of Michel (1974) important results have been published by Sturner (1993), Sturner & Dermer (1994), Sturner et al. (1995), Sturner & Dermer (1995), and Sturner (1995). Results concerning the Ruderman & Sutherland model (1975) have been published by Xia et al. (1985), Daugherty & Harding (1989), Chang (1995), Zhang & Qiao (1996), and others.

Zhang & Qiao (1996) compared inverse Compton scattering (ICS) with curvature radiation (CR) under the condition of gap sparking initiated by pair cascading in the strong magnetic field. Both reduce the height of the gap and the end energy of the electrons. Zhang & Qiao found in some cases the ICS much more important than the CR.

Among the publications based on the acceleration model of Michel (1974) the most recent and most extension work of Sturner (1995) used Monte Carlo simulations to calculate the energy transfer caused by ICS. Additionally he investigated CR and triplet pair production. The calculations revealed ICS as the dominant energy loss process for electron energies γ below a few $\times 10^6$. Above this threshold energy loss by CR dominates whereas triplet pair production was generally found to be unimportant (for typical gamma-ray pulsar parameters), except for very low electron energies with $\gamma \cong 1$.

Using Monte Carlo Methods Sturner calculated the limiting energy of electrons for two magnetic field strength (3.5×10^{12} G and 1.58×10^{13} G) and four temperatures between 2.0 and 3.5×10^6 K. Additionally, he fixed the rotation period of the neutron star to 0.150 seconds.

In this paper, we present an analytical treatment of the ICS problem including CR in the case of Michel's acceleration model and show results of numerical integrations of the developed differential equations. The anisotropy of the distribution of the thermal photons originating from the hot thermal cap is explicitely considered. The relevant parameters like magnetic field strength, thermal temperature of the hot polar cap and rotation period of the neutron star have been varied within a wide range of pulsar parameter values. In addition, we briefly discuss to what extent our results are relevant for other polar cap acceleration models, like the one described by Arons & Scharlemann (1979) which explicitly considers the effect of the divergence of the magnetic field lines or the model of Muslimov & Tsygan (1992) which describes the influence of the general relativistic frame dragging effect on the acceleration field.

2. Theory of relativistic inverse Compton scattering

For the sake of completeness we summarize in Sects. 2.1 and 2.2 the basic formulars describing the relativistic non–resonant and resonant inverse scattering processes.

Send offprint requests to: R. Supper
Correspondence to: ros@mpe.mpg.de

2.1. Non–resonant inverse Compton scattering

Let us begin with Thomson case without a magnetic field[1]. The average rate of photons scattered by relativistic electrons is given (e.g. Feenberg & Primakoff, 1948) by

$$\frac{dN}{dt} = c \int_0^\infty \int_0^{4\pi} n(\epsilon,\theta)\,(1-\beta\cos\theta)\,\sigma^*(\epsilon^*)\,d\Omega\,d\epsilon\,, \qquad (1)$$

where ϵ denotes the energy of the infalling photons, θ the angle between the moving direction of the electron in the laboratory frame and the direction of the infalling photon stream, $n(\epsilon,\theta)$ gives the number of infalling photons per unit volume dV, energy range $d\epsilon$, and solid angle element $d\Omega$, and finally σ represents the cross section. Stared letters denote quantities in the electron rest frame, unstared letters in the laboratory frame. Therefore, $\epsilon^* = \gamma(1-\beta\cos\theta)\epsilon$. As we are not interested in the rate of scattered photons but in the amount of energy transfer from an electron to photons, we have to express $\sigma^*(\epsilon^*)$ explicitly which results in

$$\frac{dE}{dr} = -\int_0^\infty \int_0^{4\pi} n(\epsilon,\theta)\,(1-\beta\cos\theta)\,d\Omega\,d\epsilon \times \int_0^{4\pi} \sigma^*(\epsilon^*,\chi^*)\,(\epsilon'-\epsilon)\,d\Omega'^*\,, \qquad (2)$$

for the differential energy loss of the electron per moving unit $dr = c\,dt$. The relation between the photon energies ϵ and ϵ' before and after Thomson scattering can be found in text books (e.g. Jackson, 1998, p. 696):

$$\epsilon' = \frac{(1-\beta\cos\theta)\,\epsilon}{1-\beta\cos\theta' + \frac{\epsilon}{m_e\,c^2}\,(1-\cos\chi)}\,, \qquad (3)$$

with m_e the rest mass of the electron, θ' the angle between the direction of the scattered photon and the moving direction of the electron, and χ the scattering angle, both angles in laboratory frame.

Taking a closer look at the cross section we have to distinguish between Thomson case and Klein–Nishina case i.e., between $\epsilon^* = \gamma(1-\beta\cos\theta)\epsilon \ll m_e\,c^2$ and $\epsilon^* \gg m_e\,c^2$. Following Feenberg and Primakoff (1948) we are now able to approximate the third integral in Eq. (2). With this and a change in the order of integration we come out with

$$\frac{dE^{ICS}}{dr} \cong -\sigma_T \int_0^{4\pi} (1-\beta\cos\theta)\,d\Omega \int_0^{\epsilon(\theta)} n(\epsilon,\theta)\,\Delta E^{(1)}\,d\epsilon - \frac{3}{4}\sigma_T \int_0^{4\pi} (1-\beta\cos\theta)\,d\Omega \times \int_{\epsilon(\theta)}^\infty n(\epsilon,\theta)\,\frac{m_e c^2}{2\epsilon^*}\,\ln\left(1+\frac{2\epsilon^*}{m_e c^2}\right)\,\Delta E^{(2)}\,d\epsilon\,. \qquad (4)$$

Here, $\sigma_T = 8\pi/3(e^2/m_e c^2)^2$ is the Thomson cross section, $\epsilon(\theta) \equiv m_e c^2/2\gamma(1-\beta\cos\theta)$ denotes the change from Thomson case to Klein–Nishina case, and the quantities

$$\Delta E^{(1)} = \frac{\gamma\,\epsilon^*}{1+\epsilon^*/m_e c^2}\,, \qquad (5)$$

$$\Delta E^{(2)} = \gamma\,m_e c^2 \times \left[1 - \frac{2\epsilon^*/m_e c^2}{(1+2\epsilon^*/m_e c^2)\ln(1+2\epsilon^*/m_e c^2)}\right] \qquad (6)$$

are approximately the average energy loss of the primary in a single Compton collision for $2\epsilon^* < m_e c^2$ and $2\epsilon^* > m_e c^2$, respectively.

2.2. Resonant inverse Compton scattering

In the presence of a (strong) magnetic field the cross section for inverse Compton scattering has a resonance when the Doppler shifted frequency of the infalling photon equals the gyro–resonance frequency of the electron in its rest frame. The later one can be written as

$$\omega^*_{res} = \frac{e\,B^*}{m_e c}\,, \qquad (7)$$

where B^* represents the strength of the magnetic field at the location of the electron in its rest frame. The Doppler shifted energy of the incoming photon is in resonance with the gyrating electron if

$$\epsilon_{res} = \frac{\hbar\,e\,B(r)}{\gamma\,(1-\beta\cos\theta)\,m_e c} \qquad (8)$$

in the laboratory frame (here we made use of the fact, that electrons in pulsar magnetospheres travel along the magnetic field lines, which leads to $B^* = B(r)$).

For a description of the resonance we use the Breit–Wigner formula. In general, the maximum cross section within the resonance can be expressed as

$$\sigma_{res} = \frac{\sigma_T}{\mu^2\,\omega^2_{res}} \qquad (9)$$

with the relaxation time

$$\mu = \frac{2}{3}\,\gamma\,\frac{e^2}{m_e c^3}\,, \qquad (10)$$

both formulated in the laboratory frame.[2] The width of the Breit–Wigner resonance is described by

$$\Delta\omega = \mu\,\omega^2_{res}\,. \qquad (11)$$

We note, that the expression

$$\sigma_{res}\,\Delta\omega = \frac{\sigma_T}{\mu} \qquad (12)$$

[1] In what follows we do not consider effects of polarization of the electromagnetic wave. A detailed discussion of polarization can be found e.g. in Kardashev et. al. (1984). The effect on intensities is about a factor of two.

[2] Again, we neglect effects due to polarization. Also the change of the cross section due to the incident angle θ is suppressed. This is justified by the results which are dominated by the photon flux with θ around 0°. For a description of the influence of the incident angle on the cross section see Mitrofanov & Pavlov (1981).

is independent on the magnetic field strength.

To find a similar expression to Eq. (4) in the case of resonant scattering we approximate the integration over $d\epsilon$ by substituting it with a multiplication of the maximum resonant cross section σ_{res} with the width $\Delta\omega = \Delta\epsilon/\hbar$ of the resonance. We find using Eq. (12):

$$\frac{dE^{RICS}}{dr} \cong -\hbar\,\frac{\sigma_T}{\mu}\int_0^{4\pi}(1-\beta\cos\theta)\,n(\epsilon,\theta)\times \tag{13}$$
$$\begin{cases} \Delta E^{(1)}_{(\epsilon_{res})}\,d\Omega & : \quad \epsilon_{res} \le \epsilon(\theta) \\ \frac{3}{4}\frac{m_e c^2}{2\epsilon^*}\,\ln\left(1+\frac{2\epsilon^*}{m_e c^2}\right)\,\Delta E^{(2)}_{(\epsilon_{res})}\,d\Omega & : \quad \epsilon_{res} > \epsilon(\theta) \end{cases}$$

Here, ϵ_{res} has to be taken from Eq. (8), $\epsilon(\theta)$ is mentioned below Eq. (4), and $\Delta E^{(1/2)}_{(\epsilon_{res})}$ come out of Eqs. (5) and (6) with $\epsilon^* \equiv \gamma\,(1-\beta\cos\theta)\,\epsilon_{res}$.

3. The thermal photon distribution

To compute Eq. (4) and (13) we need an expression for the differential photon distribution $n(\epsilon,\theta)$ of the thermal radiation from the hot polar cap of the neutron star. For the sake of simplicity we regard the symmetrical case of an electron sitting centered and above the polar cap at a height d. Further, let us assume a homogeneous and isotropic emission from a hot thermal cap. We consider two source geometries:

(a) The thermal photons come from the polar cap bordered by the open field lines (see below). This corresponds to the case where the surface is heated by the particle current.
(b) The photons originate from a larger area around the magnetic pole, e.g. $r_{tc} = 10^5$ cm. This corresponds to the case of internal heating.

The polar cap radius (case (a) above) in the standard model of an aligned rotator is given by:

$$r_{pc} = \left(\frac{\Omega\,a^3}{c}\right)^{1/2}, \tag{14}$$

with a the neutron star radius and $\Omega = 2\pi/P$ the angular velocity of the pulsar.

For the photon spectrum we use a black body model. Therefore, the energy flux per energy element $d\epsilon$ and solid angle element $d\Omega$ at any surface point within the thermal cap can be written as

$$W_\epsilon = \frac{\epsilon^3}{(2\pi\hbar)^3\,c^2\,\left(e^{\epsilon/kT}-1\right)}\,. \tag{15}$$

If $s = s(d,\vartheta)$ is the distance between the electron and the considered emission point at the thermal cap and ϑ is the angle between s and d, we can write for the flux density at the position of the electron and coming from the direction ϑ

$$dF_\epsilon(\vartheta) = \frac{W_\epsilon\,dA}{s^2} = 2\,\pi\,W_\epsilon\frac{\sin\vartheta}{\cos(\vartheta+\psi)}\,d\vartheta\,, \tag{16}$$

where dA is a differential (ring–)surface element of the thermal cap and ψ denotes the opening angle of this ring–element seen from the center of the neutron star.

As we consider a rotational symmetric situation we can identify the angle ϑ with the angle θ in Sect. 2 and therefore can write for the angular photon density $n(\epsilon,\theta)$

$$n(\epsilon,\theta) = \frac{1}{c\,\epsilon}\frac{dF_\epsilon(\theta)}{d\theta} = W'_\epsilon \times g(d,\theta)\,, \tag{17}$$

with W'_ϵ following from Eq. (15)

$$W'_\epsilon = \frac{\epsilon^2}{(2\pi\hbar\,c)^3\,\left(e^{\epsilon/kT}-1\right)} \tag{18}$$

and the geometric term

$$g(d,\theta) = 2\,\pi\frac{\sin\theta}{\cos(\theta+\psi)}\,, \tag{19}$$

with $\psi = \arcsin(\sin\theta\,s/a)$.

The maximum value allowed for θ is given either by the border of the hot thermal cap or (for small values of d) when s equals the tangent line from the electron to the neutron star (i.e. when the border of the cap is behind the horizon). The first case is expressed by

$$\theta_{tc} = \arctan\left(\frac{r_{tc}}{d}\right)\,, \tag{20}$$

with r_{tc} the radius of the hot thermal cap (for case (a) equal to r_{pc} given by Eq. (14), for case (b) set to $r_{tc} = 10^5$ cm) and the second case is expressed by

$$\theta_T = \arcsin\left(\frac{a}{d+a}\right)\,. \tag{21}$$

To compute expression (17) θ has to be always smaller than θ_{tc} (20) and θ_T (21).

We note that Eq. (17) for the differential photon distribution is physically equivalent to the one of Dermer (1990).

4. The differential equation for acceleration and damping of an electron

We are now able to give a closed expression in form of a differential equation of the acceleration and damping processes an electron undergoes within a neutron star magnetosphere. For the acceleration we use the model of Goldreich & Julian (1969) and the conditions of Michel (1974). In this model a linear acceleration for the electrons is assumed within an acceleration length equal to the polar cap radius and up to a maximum value of

$$\gamma_{max} = \left(\frac{4\,e\,B\,a^3\,\Omega^2}{m_e c^4}\right)^{1/2}\,. \tag{22}$$

With this we obtain a natural scale length for an electron to receive kinetic energy in the order of its rest energy $m_e c^2$

$$\lambda = \left(\frac{m_e c^3}{4\,e\,\Omega\,B}\right)^{1/2}\,. \tag{23}$$

Therefore, the acceleration can be described by the differential equation

$$\frac{d\gamma^{acc.}}{dr} = \begin{cases} \frac{1}{\lambda} & : \quad r \le r_{pc} \\ 0 & : \quad r > r_{pc}\,, \end{cases} \tag{24}$$

with λ and r_{pc} given in Eq. (23) and (14) respectively.

Additionally, we include energy loss by curvature radiation in our calculations which is given by (e.g. Jackson, 1998, p. 667):

$$\frac{dE^{CR}}{dr} = \frac{2}{3}\frac{e^2}{\rho^2}\beta^3\gamma^4\,. \tag{25}$$

For our calculations we set the curvature radius $\rho = 10^7$ cm, typical for the magnetic field line curvature at the rim of the thermal cap with $r_{pc} = 10^5$ cm (see also Sturner 1995).

Finally, using the expressions we derived in Sect. 2 for the damping processes by nonresonant and resonant inverse Compton scattering (ICS and RICS, respectively) we come out with the differential equation for the discussed model:

$$\frac{d\gamma}{dr} = \frac{d\gamma^{acc.}}{dr} + \frac{1}{m_e c^2}\left(\frac{dE^{ICS}}{dr} + \frac{dE^{RICS}}{dr} + \frac{dE^{CR}}{dr}\right). \tag{26}$$

The here used quantities are given in Eqs. (24), (4), (13), with the use of (17), and (25).

5. Computation and results

To solve Eq. (26) we used various numerical methods. For the differential equation itself a Runge–Kutta algorithm fourth order was used. All calculations were repeated several times with different step sizes to check for the stability of the solution. For the integrations a recursive Simpson method was performed and all results were proofed by substituting the Simpson method for a Romberg algorithm with adaptive step size.

The two diagrams in Fig. 1 and Fig. 2 show our results for parameter settings used by Sturner (1995) in his Monte Carlo simulations, i.e. $P = 0.150$ s, $B = 3.5 \times 10^{12}$ Gauss for Fig. 1 and $B = 1.58 \times 10^{13}$ Gauss for Fig. 2, respectively. In both cases 10^5 cm is used for the radius of the hot thermal cap, whereas for the height of the acceleration zone r_{pc} is used as given in formula (14). From relation (22) follows $\gamma_{max} = 1.26 \times 10^5$ and $\gamma_{max} = 2.7 \times 10^5$, respectively, for the maximum Lorentz factor of an electron being fully accelerated without any damping. From this and both figures it is obvious that damping caused by inverse Compton scattering of thermal photons does not have any significant effect for temperatures below 100 eV, in agreement with the results from Sturner (1995). For temperatures between 100 eV and 200 eV we find a stronger damping effect during acceleration than Sturner did (for a discussion see Sect. 6). Nevertheless, this is not relevant for most pulsar magnetosphere models because they only make use of the maximum Lorentz factor above the acceleration zone.

Fig. 3 compares results of the calculations including (solid lines) and excluding (dashed lines) the non–resonant part of the ICS (dE^{ICS}/dr in Eq. (26)). For each situation the upper line

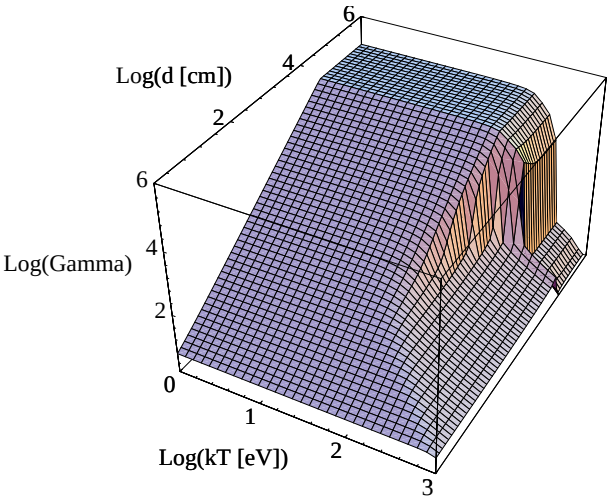

Fig. 1. Electron Lorentz factor $\gamma(d, kT)$ as a function of height d (above the polar cap surface) and the thermal temperature kT of the hot polar cap. Here, for a comparison we used the same pulsar parameter settings like Sturner & Dermer (1995): $P = 0.150$ s, $B = 3.5 \times 10^{12}$ Gauss, and $r_{tc} = 10^5$ cm for the thermal cap radius.

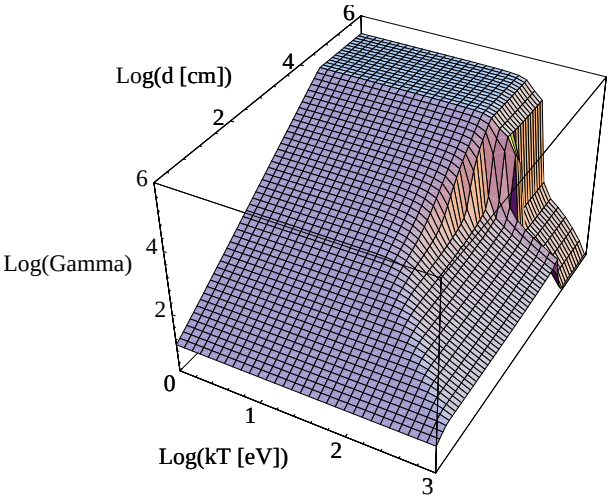

Fig. 2. The same like Fig. 1 but for $B = 1.58 \times 10^{13}$ Gauss.

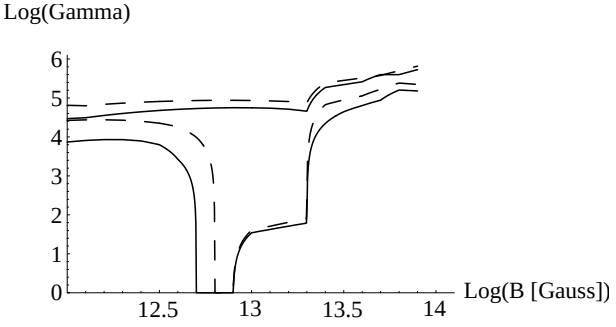

Fig. 3. Electron end energies $\gamma(B)$ as a function of magnetic field strength for two different pulsar rotation periods. The dashed lines show the influence of resonant ICS whereas the solid lines are for the total, resonant and non–resonant ICS. In each case the upper line results from calculations with $P = 0.100$ s the lower from $P = 0.150$ s. The other parameter settings are: $kT = 300$ eV and $r_{tc} = 10^5$ cm.

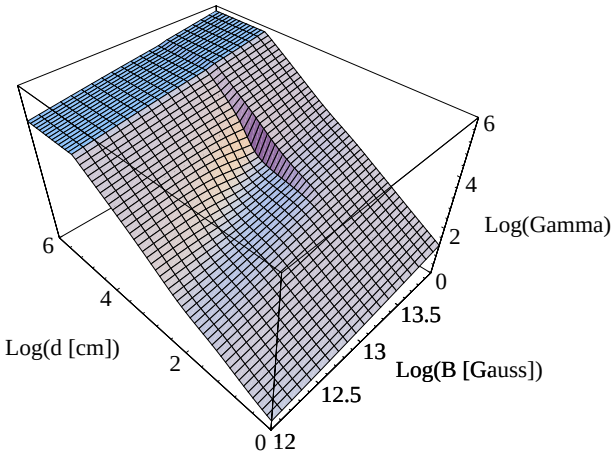

Fig. 4. Electron Lorentz factor $\gamma(d, B)$ as a function of height d above the polar cap surface and magnetic field strength B for $kT = 100\,\mathrm{eV}$. The pulsar rotation period is set to $P = 0.150\,\mathrm{s}$ and the radius of the hot thermal cap is set to $r_{tc} = 10^5\,\mathrm{cm}$.

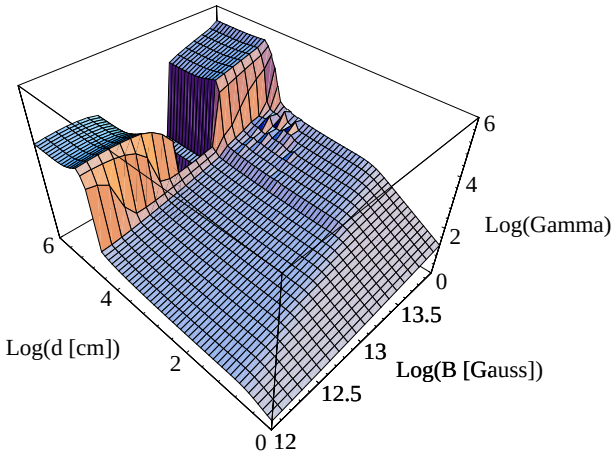

Fig. 5. The same like Fig. 4 but for $kT = 300\,\mathrm{eV}$.

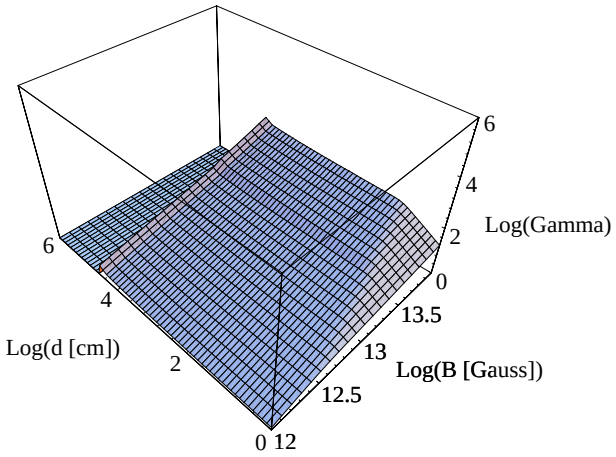

Fig. 6. The same like Fig. 4 but for $kT = 1000\,\mathrm{eV}$.

shows the electron end energies $\gamma(B)$ with a pulsar rotation period $P = 0.100\,\mathrm{s}$, the lower lines represents the results for $P = 0.150\,\mathrm{s}$. For all calculations $kT = 300\,\mathrm{eV}$ and $r_{tc} = 10^5\,\mathrm{cm}$. As can be seen just from this figure, neglecting the non–resonant part of the ICS may change the results significantly.

For a complete overview we present in Figs. 4 to 6 the developement of the electron energy $\gamma(d, B)$ as a function of height d above the polar cap and magnetic field strength B for three thermal temperatures $kT = 100\,\mathrm{eV}$, $300\,\mathrm{eV}$, and $1000\,\mathrm{eV}$, respectively. For all three cases, the pulsar rotation period is set to $P = 0.150\,\mathrm{s}$ and the radius of the hot thermal cap to $r_{tc} = 10^5\,\mathrm{cm}$.

In the situation with $kT = 100\,\mathrm{eV}$ (Fig. 4) damping by ICS has only a slight influence on the electron energy within a part of the acceleration zone and for magnetic field strengths around $B = 10^{13}$ Gauss. The end energy above the acceleration zone remains nearly uneffected.

In the case of $kT = 300\,\mathrm{eV}$ (Fig. 5) and for a wide range of magnetic field strengths damping by ICS prevents the electrons from being fully accelerated within the acceleration zone. Only below $10^{12.5}$ Gauss and above $10^{13.5}$ Gauss the electrons recover to end energies approximately half an order below the undamped situation (compare to Fig. 4). Between these magnetic field strengths, the electrons completely lose their energy.

For $kT = 1000\,\mathrm{eV}$ (Fig. 6) the electrons are not only braked within the acceleration zone but also above. As a result, only low energy electrons can be found within the magnetosphere above the acceleration zone (for the considered magnetic field strengths).

Finally, Figs. 7 to 9 show the end energies the electrons can reach above the acceleration zone as a function of pulsar rotation period P and magnetic field strength B, again for the three thermal temperatures $kT = 100\,\mathrm{eV}$, $300\,\mathrm{eV}$, and $1000\,\mathrm{eV}$, respectively. For all three cases, the radius of the hot thermal cap is set to $10^5\,\mathrm{cm}$. With increasing temperature the plateau of damped electrons enlarges to smaller rotation periods and to a wider range of magnetic field strengths. Nevertheless, as can clearly be seen, millisecond pulsars are not effected at all (even for magnetic field strengths around $B = 10^8$ Gauss, not shown in these figures).

6. Discussion

All calculations base on Eq. (26), which neglects energy loss due to triplet pair production. Sturner (1995) showed that ICS dominates over all other energy loss effects when $\gamma < 10^6$. This is exactly the energy range we are interested in here. Electron bunching (to produce coherent radio emission by curvature radiation) could decrease the range of validity of our calculations, because energy losses by curvature radiation could then become much more important. On the other hand, the latter depends strongly on the assumed curvature radius of the magnetic field lines (see Eq. (25)). The value of $\rho = 10^7\,\mathrm{cm}$ for the curvature radius used in the calculations corresponds to a typical curvature of the magnetic field lines at the rim of the thermal cap. Because this radius increases (and therefore energy loss by CR decreases) from the rim to the center of the polar cap, the mean value of the CR power is less by at least one order

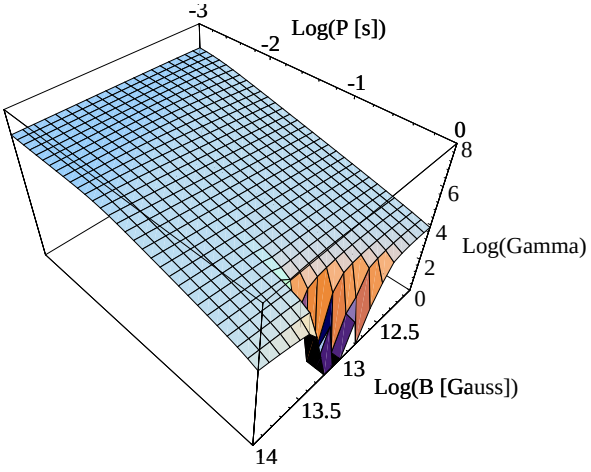

Fig. 7. End electron Lorentz factor $\gamma(P, B)$ as a function of pulsar rotation period P and magnetic field strength B for $kT = 100\,\mathrm{eV}$. The radius of the hot thermal cap is set to $r_{tc} = 10^5$ cm.

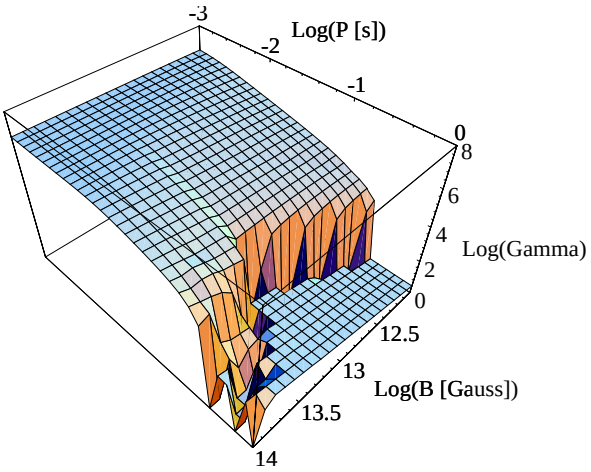

Fig. 8. The same like Fig. 7 but for $kT = 300\,\mathrm{eV}$.

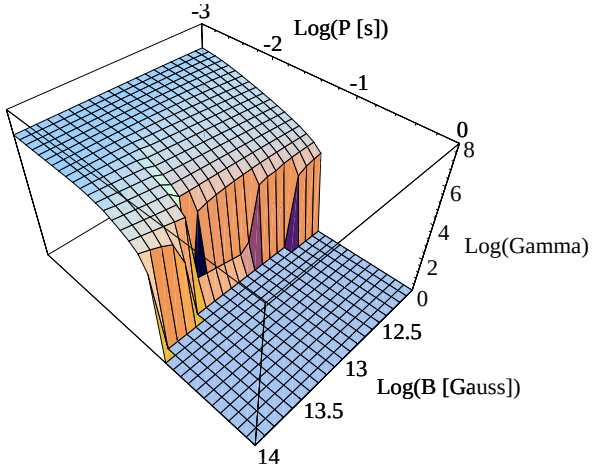

Fig. 9. The same like Fig. 7 but for $kT = 1000\,\mathrm{eV}$.

which turns out our calculations as being conservative. The effect of the energy loss by CR can be seen in Figs. 7 to 9, where it clearly restricts the maximum end energy of the electrons to a few $\times 10^6$ (in the edge of the diagrams with high values for B and low values for P).

In Sect. 5 we mentioned a difference in Lorentz factors within the acceleration zone for the situation with kT between 100 eV and 200 eV when compared to the values of Sturner (1995), whereas the final Lorentz Factor above the acceleration zone is comparable to their results. In Sect. 2 we mentioned that our computations do not include photon polarization effects and also no changes of the resonant cross section due to different incident angles. Both neglects result in a small overestimation of the damping by inverse Compton scattering. Therefore, it is understandable, that our results show a stronger damping in the acceleration zone compared to the results of Sturner. This difference vanishes when the electrons approach the top of the acceleration zone because RICS plays a minor rule there (for the considered magnetic field strength). Another point is, that we consider the magnetic field to be proportional to r^{-3} and therefore do not include its dependence on the azimute angle. As a consequence, we regard the electrons as moving radially outward. This is surely a good approximation, because the dominant damping effect takes place up to a height of 10^{-2} of the neutron star radius, where the magnetic field lines have a negligible curvature.

On the other hand, the radius of the hot thermal cap r_{tc} has a large influence on the results. All calculations shown in the figures of this paper refer to the case of a large hot thermal cap (case (b) in Sect. 3, $r_{tc} = 10^5$ cm). If we use case (a) and set $r_{tc} = r_{pc} = 3.7 \times 10^4$ cm, at the top of the acceleration zone the maximum angle for the infalling photons decreases from $72°$ to $45°$, which results in a weaker damping. Additionally, the area of the polar cap is smaller by a factor of $\cong 7$. Both effects together lead to higher values for the end energy of the accelerated electrons. In the case of low magnetic field strengths ($B \cong 10^{12}$ Gauss) the electrons lose their energies at lower heights, where a different size of the hot thermal cap is of negligible influence. But in the situation of high magnetic field strengths ($B \cong 10^{13}$ Gauss) and high temperatures ($kT \cong 200$ eV) this effect can change the end energy of the electrons by three orders. On the other hand, increasing r_{tc} higher than 3×10^5 cm has no further influence, because the rim of the thermal cap is then beyond the horizon. Therefore, we chose $r_{tc} = 10^5$ cm for our calculations as a reasonable value.

In Sect. 5 we already stressed the important effect of the non–resonant part of the ICS (dE^{ICS}/dr in Eq. (26)) on the electron end energies (see Fig. 3). The non–resonant ICS is often characterized as being negligible in comparison with the resonant part (e.g. Sturner 1995, Zhang & Qiao 1996, and others). This is fairly true for a wide range of parameters but it is obviously wrong for parameter settings used in Fig. 3, where for magnetic field strengths arround $B \cong 5 \times 10^{12}$ Gauss and pulsar rotation periods of $P = 0.150\,\mathrm{s}$ the electron end energies are clearly affected by non–resonant ICS. These parameter values are absolutely typical for neutron stars.

Figs. 7 to 9 show the (expected) fact, that ICS has no influence on the end energies of electrons within the magnetosphere of millisecond pulsars. For standard pulsars ($P > 0.1$ s) the situation strongly depends on temperature and magnetic field strength. Here, for any model of pulsar magnetospheres ICS has to be taken into account.

Our results have been derived assuming Michel's acceleration model. In the following we want to discuss briefly to what extent they are relevant for other polar cap acceleration models which use higher acceleration potentials resulting from either stronger electric fields or larger acceleration heights, or both. E.g. Arons & Scharlemann's (1979) acceleration scheme considers the effect of the divergence of the magnetic field lines which produces changes in the local Goldreich–Julian density and a consequent acceleration over a much larger length of the open field lines. In addition to this effect is the general relativistic frame dragging effect of Muslimov & Tsygan (1992) which also produces an additional acceleration.

In order to check on the effects of electron braking under such conditions we (1) increased the acceleration field in steps up to one hundred times over the value used within the model of Michel and we (2) increased the height of the acceleration zone by factors up to ten. In the first case we found curvature radiation as becoming increasingly important. It limits the end energies γ of the electrons to a few times 10^6. The energy loss due to ICS did not increase. In the second case we found the electrons being accelerated within the additional upper part of the acceleration zone without any significant damping. This is because at these heights the flux density of the thermal photons is already too low and also the angles of the infalling photons are too small to cause a significant ICS braking effect. The pair cascades occuring in the models of Arons & Scharlemann (1979) and Muslimov & Tsygan (1992) start at a height of about one neutron star radius. As pointed out above in that region the braking by thermal photons is already small for particles travelling along the field lines. We have not investigated the additional braking occuring due to the angular divergence of pair electrons. Concerning this point, e.g. see Zhang & Harding (2000). We want to point out, within the inner magnetosphere up to one neutron star radius in height our results concerning the energy loss by ICS remain valid, more or less independent of the choosen acceleration model.

7. Conclusions

In the case of low temperatures ($kT \ll 100$ eV) of the hot thermal cap, for a wide range of magnetic field strengths B and rotation periods P, inverse Compton scattering (resonant and nonresonant) of thermal photons by accelerated electrons is not able to significantly lower the final maximum Lorentz factor of the electrons leaving the acceleration zone described by the model of Michel (1974). For (standard) pulsars with $P > 0.1$ s, temperatures around $kT = 100$ eV, and magnetic field strengths between $10^{12.5}$ Gauss and $10^{13.5}$ Gauss a substantial damping occurs. This effect extends over a wider range of magnetic field strengths in the case of $kT > 200$ eV.

The situation within the acceleration zone is more complicated. Here a large region exists, where electrons can not be accelerated above Lorentz factors of $\gamma \cong 10^1 ... 10^2$, but recover to high energies before they reach the end of the acceleration zone. Therefore, high end energies of the electrons near the theoretical maximum energy do not guarantee for a linear acceleration within the acceleration zone.

Although the cross section for non–resonant ICS is much lower than for the resonant ICS, neglecting the contribution of non–resonant ICS may lead to wrong results for parameter settings (e.g. $B = 5 \times 10^{12}$ Gauss and $P = 0.150$ s) which are absolutely typical for standard neutron stars.

For millisecond pulsars no braking due to inverse Compton scattering occurs, as expected, as long as magnetic dipole fields are considered. The final maximum Lorentz factor as well as the intermediate Lorentz factors during acceleration are not affected by any significant damping except for the first few centimeters near the neutron star surface.

The results reported here concerning the energy loss due to ICS is found to remain valid up to a height of the inner magnetosphere of approximately one neutron star radius, independent of the choosen acceleration model.

Acknowledgements. We would like to thank the anonymous referee for useful comments. RS is supported by the Deutsches Zentrum für Luft– und Raumfahrt (DLR).

References

Arons J., Scharlemann E.T., 1979, ApJ 231, 854
Chang H.K., 1995, A&A 301, 456
Daugherty J.K., Harding A.K., 1989, ApJ 336, 861
Dermer C.D., 1990, ApJ 360, 197
Feenberg E., Primakoff H., 1948, Phys. Rev. 73, No. 5, 449
Goldreich P., Julian W.H., 1969, ApJ 157, 869
Jackson J.D., 1998, Classical Electrodynamics 3, John Wiley & Sons
Kardashev N.S., Mitrofanov I.G., Novikov I.D., 1984, AZh 61, 1113
Michel F.C., 1974, ApJ 192, 713
Mitrofanov I.G., Pavlov G.G., 1981, MNRAS 200, 1033
Muslimov A.G., Tsygan A.I., 1992, MNRAS 255, 61
Ruderman M.A., Sutherland P.G., 1975, ApJ 196, 51
Sturner S.J., 1995, ApJ 446, 292
Sturner S.J., 1993, Ph.D. Thesis, Rice University
Sturner S.J., Dermer C.D., 1994, ApJ 420, L79
Sturner S.J., Dermer C.D., 1995, Adv. Space. Res. Vol. 15, No. 5, 80
Sturner S.J., Dermer C.D., Michel F.C., 1995, ApJ 445, 736
Xia X.Y., Qiao G.J., Wu X.J., Hou Y.Q., 1985, A&A 152, 93
Zhang B., Harding A.K., 2000, ApJ, accepted
Zhang B., Qiao G.J., 1996, A&A 310, 135